The Trajectory Analysis of Bevel Planetary Gear Trains

Chen-Chou Lin

Lung-Wen Tsai

Mechanical Engineering Department
and Systems Research Center,
University of Maryland,
College Park, MD 20742

In this paper, the trajectory of bevel planetary gear trains has been studied. The parametric equations of trajectory are derived. It is shown that the trajectory generated by a tracer point on the planet of a bevel planetary gear train is analogous to that of a spur planetary gear train. Two cases, gear ratio equal to one and two, are presented in detail including the geometric description, plane of symmetry, extent of trajectory, number of nodes (cusps) and their locations. The criteria for the existence of cusps are verified algebraically, and interpreted from geometrical point of view.

1 Introduction

In the theory of Kinematics of Mechanisms, trajectories generated by planetary gear trains form an important family of curves, known as Epitrochoids or Hypotrochoids, depending on whether the gearing is external or internal (Lawrence, 1972; and Hunt, 1978). If the tracer point is on the pitch circle of the planet gear, the curves are called Epicycloids or Hypocycloids. Knowledge of planar epicyclic curves dates back to two thousand years ago, when ancient astronomer Hipparchos (180–125 B.C.) used epicycles to describe the paths of planets. Throughout the history of science and technology, these curves also found applications in mechanics, optics, architecture, mechanisms, etc. (Brieskorn, 1986; Jensen, 1965; Pollitt, 1960; and Spragg and Tesar, 1971).

In this paper, the geometry of trajectories generated by a tracer point on the planet of bevel planetary gear trains is studied. This study serves as a precursor to the workspace analysis of a new class of gear-coupled, three DOF (Degrees Of Freedom), four-jointed wrist mechanisms. Before further discussion, it is helpful to review briefly the trajectories generated by a spur planetary gear train because of the analogy between them.

Figure 1 shows a one-DOF spur planetary gear train, which consists of three links, two turning pairs, and one gear pair. The input link of the system is the carrier (link 2). The sun gear is fixed to the ground (link 1), while the planet (link 3) revolves around the sun gear as the carrier rotates. Let the radii of the sun and planet gears be r_s and r_p, respectively. Then, the length of the carrier, l_2, is equal to $r_s + r_p$. Let the distance from the tracer point to the center of the planet gear be l_3 and let the initial position be as shown in Fig. 1 (zero phase angle). Then the position of the tracer point can be described by the following parametric equations:

$$x = l_2 c\theta_2 + l_3 c[(1 + r_s/r_p)\theta_2]$$
$$y = l_2 s\theta_2 + l_3 s[(1 + r_s/r_p)\theta_2] \quad (1)$$

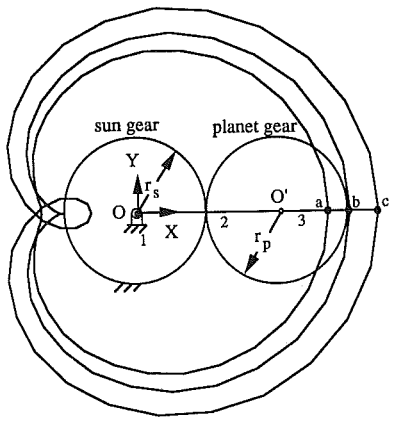

Fig. 1 The limacons trace by planar planetary gear trains (n = 1), where l_3 = 0.7, 1, and 1.4 for tracer points a, b, and c, respectively

where θ_2 is the inclination of OO' (link 2), and where c denotes the cosine function and s the sine function.

Let the radii of both gears be one, and the lengths of l_3 for tracer points a, b, and c, be 0.7, 1.0, and 1.4, respectively. Then the trajectory traced by point c, which lies outside the pitch circle of the planet gear, has a node, while the trajectory traced by point b, which lies on the pitch circle of the planet gear, has a cusp, as shown in Fig. 1. The curve is called a *limacon* when r_s/r_p = 1, and is called a *cardioid* when r_s/r_p = l_3/r_p = 1. The geometric properties of limacons and cardioids can be found in McCarthy (1945), or Butchart (1945). For other ratios of r_s/r_p and l_3/r_p, see Lawrence (1972), for the shape of curves.

2 Parametric Equations of the Trajectory

Figure 2 shows the schematic of a bevel planetary gear train. The trajectory generated by a tracer point on the planet gear lies on a sphere centered about point O, the common apex of

Contributed by the Power Transmission and Gearing Committee for publication in the JOURNAL OF MECHANICAL DESIGN. Manuscript received October 1990. Associate Technical Editor: D. G. Lewicki.

the pitch cones formed by the sun and planet gears. The link coordinate systems are defined according to the D-H (Denavit-Hartenberg, 1955) convention. The origin of each coordinate system is located at the center O. However, they have been sketched away from the center for the reason of clarity. The $(XYZ)_1$ coordinate system is fixed to the base link with the X_1-axis pointing out of the paper and the Z_1-axis pointing along the first joint axis. We have chosen the stretched out, joint axes coplanar configuration of the mechanism as the reference position, and define all the positive X-axes to be pointing out of the paper. The joint angle θ_i is the angle measured from X_{i-1} to X_i-axis about the positive Z_{i-1}-axis. The directions of the Z-axes are chosen in such a way that twist angles, α_2 and α_3, are less than π and greater than zero. The twist angle α_i is the angle measured from Z_{i-1} to Z_i-axis about the positive X_i-axis. Let α_s and α_p denote the cone angles of the sun gear and planet gear, respectively, and let $n = \sin \alpha_s / \sin \alpha_p$ be the gear ratio, then,

$$n = -\frac{\dot{\theta}_{32}}{\dot{\theta}_{12}} = \frac{\dot{\theta}_{32}}{\dot{\theta}_{21}} \tag{2}$$

where $\dot{\theta}_{ij}$ is the magnitude of the angular velocity of link i with respect to link j. In what follows, we shall use $\dot{\theta}_i$ to denote $\dot{\theta}_{i,i-1}$ for brevity.

Integrating Eq. (2), yields

$$\theta_3 = n\theta_2 + \theta_p \tag{3}$$

where $\theta_3 = \theta_{32}$ and $\theta_2 = \theta_{21}$ are the joint angles associated with links 3 and 2, respectively, and θ_p is a phase angle. For the configuration shown in Fig. 2, the phase angle θ_p is equal to zero.

The position vector $\mathbf{P}$ of a tracer point P, located on the Z_3-axis and one unit length away from the origin as shown in Fig. 2, can be expressed in $(XYZ)_1$ frame as

$$\mathbf{P} = \begin{bmatrix} c\theta_2 & -s\theta_2 c\alpha_2 & s\theta_2 s\alpha_2 \\ s\theta_2 & c\theta_2 c\alpha_2 & -c\theta_2 s\alpha_2 \\ 0 & s\alpha_2 & c\alpha_2 \end{bmatrix} \begin{bmatrix} s\theta_3 s\alpha_3 \\ -c\theta_3 s\alpha_3 \\ c\alpha_3 \end{bmatrix}$$

$$= \begin{bmatrix} c\theta_2 s\theta_3 s\alpha_3 + s\theta_2 c\theta_3 c\alpha_2 s\alpha_3 + s\theta_2 s\alpha_2 c\alpha_3 \\ s\theta_2 s\theta_3 s\alpha_3 - c\theta_2 c\theta_3 c\alpha_2 s\alpha_3 - c\theta_2 s\alpha_2 c\alpha_3 \\ -c\theta_3 s\alpha_2 s\alpha_3 + c\alpha_2 c\alpha_3 \end{bmatrix} \tag{4}$$

where θ_3 is related to θ_2 by Eq. (3). The point P will trace a curve as θ_2 varies from $-\pi$ to π.

3 Effect of the Phase Angle

We shall discuss the effect of the phase angle θ_p on the trajectory of P. Let $\theta_p = 0$, then $\theta_3 = n\theta_2$, and Eq. (4) becomes

$$\mathbf{P} = \begin{bmatrix} c\theta_2 s(n\theta_2) s\alpha_3 + s\theta_2 c(n\theta_2) c\alpha_2 s\alpha_3 + s\theta_2 s\alpha_2 c\alpha_3 \\ s\theta_2 s(n\theta_2) s\alpha_3 - c\theta_2 c(n\theta_2) c\alpha_2 s\alpha_3 - c\theta_2 s\alpha_2 c\alpha_3 \\ -c(n\theta_2) s\alpha_2 s\alpha_3 + c\alpha_2 c\alpha_3 \end{bmatrix} \tag{5}$$

Now suppose $\theta_p \neq 0$, then the new position vector $\mathbf{P}'$ becomes

$$\mathbf{P}' = \begin{bmatrix} c\theta_2 s(n\theta_2 + \theta_p) s\alpha_3 + s\theta_2 c(n\theta_2 + \theta_p) c\alpha_2 s\alpha_3 + s\theta_2 s\alpha_2 c\alpha_3 \\ s\theta_2 s(n\theta_2 + \theta_p) s\alpha_3 - c\theta_2 c(n\theta_2 + \theta_p) c\alpha_2 s\alpha_3 - c\theta_2 s\alpha_2 c\alpha_3 \\ -c(n\theta_2 + \theta_p) s\alpha_2 s\alpha_3 + c\alpha_2 c\alpha_3 \end{bmatrix} \tag{6}$$

Replacing the parameter $n\theta_2$ in Eq. (6) by $n\theta_2 - \theta_p$, and θ_2 by $\theta_2 - \theta_p/n$, yields,

$$\mathbf{P}'' = \begin{bmatrix} s(n\theta_2) c(\theta_2 - \theta_p/n) s\alpha_3 + c(n\theta_2) s(\theta_2 - \theta_p/n) c\alpha_2 s\alpha_3 + s(\theta_2 - \theta_p/n) s\alpha_2 c\alpha_3 \\ s(n\theta_2) s(\theta_2 - \theta_p/n) s\alpha_3 - c(n\theta_2) c(\theta_2 - \theta_p/n) c\alpha_2 s\alpha_3 - c(\theta_2 - \theta_p/n) s\alpha_2 c\alpha_3 \\ -c(n\theta_2) s\alpha_2 s\alpha_3 + c\alpha_2 c\alpha_3 \end{bmatrix} \tag{7}$$

Equation (7) can also be written as:

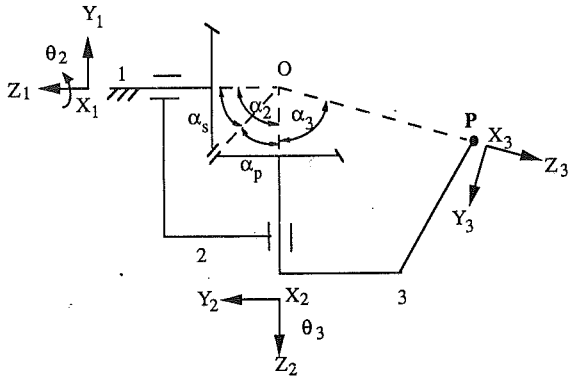

Fig. 2 A bevel planetary gear train

$$\mathbf{P}'' = \begin{bmatrix} c(\theta_p/n) & s(\theta_p/n) & 0 \\ -s(\theta_p/n) & c(\theta_p/n) & 0 \\ 0 & 0 & 1 \end{bmatrix} \times \begin{bmatrix} c\theta_2 s(n\theta_2) s\alpha_3 + s\theta_2 c(n\theta_2) c\alpha_2 s\alpha_3 + s\theta_2 s\alpha_2 c\alpha_3 \\ s\theta_2 s(n\theta_2) s\alpha_3 - c\theta_2 c(n\theta_2) c\alpha_2 s\alpha_3 - c\theta_2 s\alpha_2 c\alpha_3 \\ -c(n\theta_2) s\alpha_2 s\alpha_3 + c\alpha_2 c\alpha_3 \end{bmatrix}$$

$$= R(-\theta_p/n, \hat{\mathbf{Z}}_1)\mathbf{P} \tag{8}$$

where R denotes a rotation matrix.

Equation (8) shows that adding a phase angle has the effect of rotating the original vector and, hence, the trajectory about Z_1-axis an angle $-\theta_p/n$. Note that the shape of the trajectory is not changed under orthogonal transformation.

4 Geometry of the Trajectory, Gear Ratio $n = 1$

A geometric description of the parametric equations can help us to visualize the trajectory of P. Since θ_p only affects the orientation of the trajectory, we may assume $\theta_p = 0$ without loss of generality. For $n = 1$, Eq. (5) reduces to

$$\mathbf{P} = \begin{bmatrix} c\theta_2 s\theta_2 s\alpha_3 (1 + c\alpha_2) + s\theta_2 s\alpha_2 c\alpha_3 \\ (1 - c^2\theta_2) s\alpha_3 - c^2\theta_2 c\alpha_2 s\alpha_3 - c\theta_2 s\alpha_2 c\alpha_3 \\ -c\theta_2 s\alpha_2 s\alpha_3 + c\alpha_2 c\alpha_3 \end{bmatrix} \tag{9}$$

4.1 Geometric Description. Eliminating θ_2 from the second and third equations in Eq. (9), yields

$$\left(z + \frac{k_2}{2k_1}\right)^2 + \frac{k_3}{k_1}\left[y - \left(\frac{k_2^2}{4k_1k_3} - \frac{k_4}{k_3}\right)\right] = 0 \tag{10}$$

where

$$k_1 = c\alpha_2 + 1$$

$$k_2 = -2c\alpha_2 c\alpha_3 (1 + c\alpha_2) - c\alpha_3 s^2\alpha_2$$

$$k_3 = s^2\alpha_2 s\alpha_3$$

$$k_4 = c^2\alpha_2 c^2\alpha_3 (1 + c\alpha_2) + s^2\alpha_2 (c\alpha_2 c^2\alpha_3 - s^2\alpha_3)$$

Equation (10) represents a cylinder with a parabolic directrix in the Y-Z plane and with its elements parallel to the X-axis. The coefficient of y, (k_3/k_1), is always positive. Therefore,

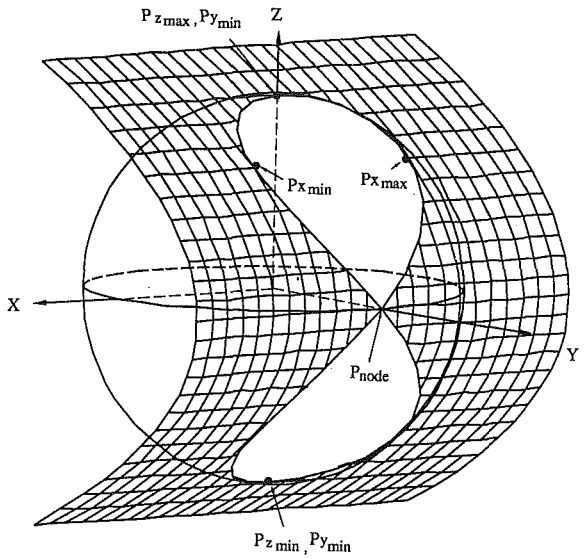

$\alpha_2 = \pi/2$ and $\alpha_3 = \pi/2$

Fig. 3 Intersection of a parabolic cylinder and a unit sphere

the directrix parabola is convex to the positive Y-axis direction. The z-coordinate of the apex is located at

$$z_a = -\frac{k_2}{2k_1} = \frac{1}{2} c\alpha_3(1 + c\alpha_2) \tag{11}$$

The sign of z_a depends on α_3. If $0 < \alpha_3 < \pi/2$, then the apex is located above the X-Y plane; if $\pi/2 < \alpha_3 < \pi$, then it is located below the X-Y plane. The y-coordinate of the apex, which is also the maximum y-coordinate of the cylinder, is given by

$$y_a = s\alpha_3 + \frac{c^2\alpha_3(1 - c\alpha_2)}{4s\alpha_3} \tag{12}$$

Summing the squares of the x, y, z components of Eq. (5), yields $x^2 + y^2 + z^2 = 1$. Hence, the trajectory of point P is the intersection of the cylinder and a unit sphere. Figure 3 shows a typical parabolic cylinder and its intersection with a unit sphere.

4.2 Extrema, Nodes, and Cusps. For the planar motion, the geometry of epitrochoids has been described in several aspects: axes of symmetry, extent of the curve, number of node(s) or cusp(s) and their location(s), etc. Similar geometric characteristics can also be used in the spherical motion. Since elements of the cylinder (Fig. 3) are parallel to the X-axis, the intersection of the cylinder with a unit sphere centered at origin is symmetric with respect to the Y-Z plane. The extend of the trajectory can be found by solving the extreme values of its x, y, and z coordinates.

Extrema of z

The extreme values of z can be found by equating the derivative of the z-component in Eq. (9) to zero, i.e.

$$\frac{dz}{d\theta_2} = s\theta_2 s\alpha_2 s\alpha_3 = 0 \tag{13}$$

From the above equation and the second-order derivative of z, we conclude that at $\theta_2 = \pi$ and $\theta_2 = 0$, z reaches its maximum z_{max} and minimum z_{min}, respectively, as shown in Fig. 3. Substituting $\theta_2 = \pi$ into Eq. (9), yields

$$\mathbf{P}_{z_{max}} = \begin{bmatrix} 0 \\ s(\alpha_2 - \alpha_3) \\ c(\alpha_2 - \alpha_3) \end{bmatrix} \tag{14}$$

Substituting $\theta_2 = 0$ into Eq. (9), yields

$$\mathbf{P}_{z_{min}} = \begin{bmatrix} 0 \\ -s(\alpha_2 + \alpha_3) \\ c(\alpha_2 + \alpha_3) \end{bmatrix} \tag{15}$$

Note that the two vectors with extreme values of z lie on the Y-Z plane, the plane of symmetry for the trajectory. Equations (14) and (15) imply that, the angle ψ_z, measured from $\mathbf{P}_{z_{max}}$ to $\mathbf{P}_{z_{min}}$ in the clockwise direction, is given by

$$\psi_z = 2(\pi - \alpha_2) \tag{16}$$

We note that the angle ψ_z is a function of α_2 only, and $\psi_z = \pi$ when $\alpha_2 = \pi/2$.

Extrema of x

The extreme values of x can be found by equating the first derivative of the x-component in Eq. (9) to zero, i.e.

$$\frac{dx}{d\theta_2} = 2u_0c^2\theta_2 + u_1c\theta_2 - u_0 = 0 \tag{17}$$

where $u_0 = s\alpha_3 + c\alpha_2 s\alpha_3$, and $u_1 = s\alpha_2 c\alpha_3$.

The solutions of Eq. (17) are

$$\theta_2 = \cos^{-1}\left(\frac{-u_1 \pm \sqrt{u_1^2 + 8u_0^2}}{4u_0}\right) \tag{18}$$

There will be four extreme values of x, if

$$-1 \le \frac{-u_1 \pm \sqrt{u_1^2 + 8u_0^2}}{4u_0} \le 1 \tag{19}$$

It can be shown that Eq. (19) is satisfied if

$$\frac{\alpha_2}{2} \le \alpha_3 \le \pi - \frac{\alpha_2}{2} \tag{20a}$$

or

$$\alpha_p \le \alpha_3 \le \pi - \alpha_p \tag{20b}$$

Equation (20) is the condition for the trajectory to have four extreme values of x. The position of $\mathbf{P}$ with extreme values of x-coordinates can be obtained by substituting the solutions of θ_2 from Eq. (18) into Eq. (9). However, they are no longer in a simple form. There are two pairs of $\mathbf{P}_{x_{max}}$ and $\mathbf{P}_{x_{min}}$ when Eq. (20) is satisfied, and $x_{min} = -x_{max}$ for each pair of extreme positions. The angle, ψ_x, between $\mathbf{P}_{x_{max}}$ and $\mathbf{P}_{x_{min}}$ is given by

$$\psi_x = 2 \sin^{-1}(x_{max}) \tag{21}$$

Points of intersection at the Y-Z plane

Equating the x-component in Eq. (9) to zero, we obtain the points where the trajectory intersect the Y-Z plane:

$$s\theta_2[c\theta_2 s\alpha_3(1 + c\alpha_2) + s\alpha_2 c\alpha_3] = 0$$

Hence,

$$\theta_2 = 0 \text{ or } \pi \tag{22a}$$

or

$$\theta_2 = \cos^{-1}\left(-\frac{s\alpha_2 c\alpha_3}{s\alpha_3(1 + c\alpha_2)}\right) \tag{22b}$$

Equation (22a) implies that the trajectory intersects the Y-Z plane at least twice at the locations where the extreme values of z occur. Equation (22b) yields two real solutions if

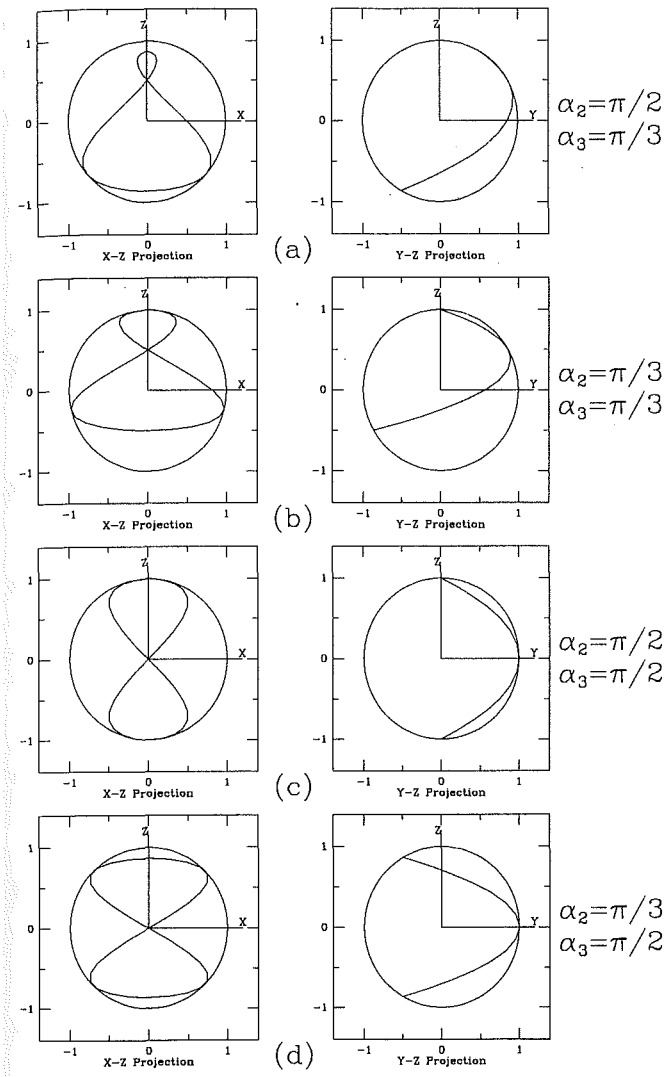

Fig. 4 Spherical limacons generated by bevel planetary gear trains (n = 1)

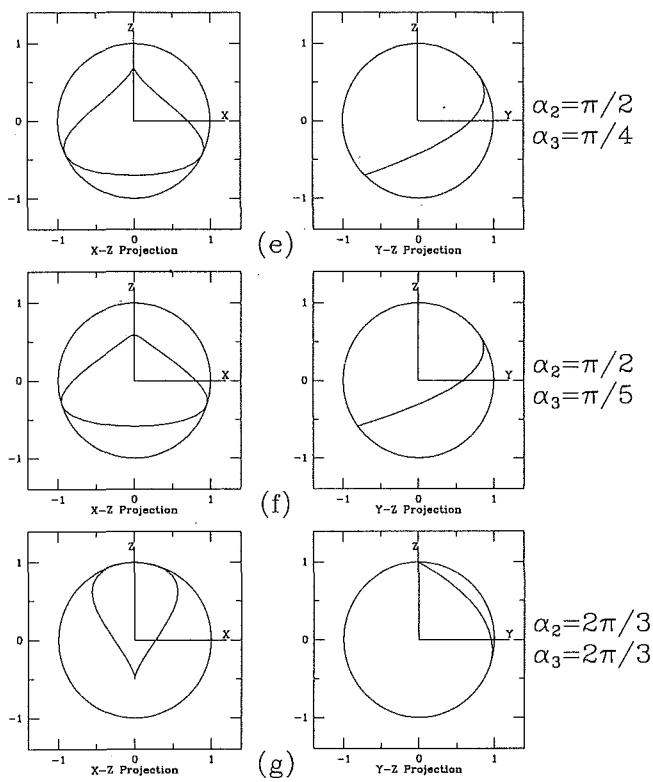

Fig. 4 (Continued)

$$-1 \le -\frac{s\alpha_2 c\alpha_3}{s\alpha_3(1+c\alpha_2)} \le 1 \tag{23}$$

It can be shown that Eq. (23) is satisfied when

$$\frac{\alpha_2}{2} \le \alpha_3 \le \pi - \frac{\alpha_2}{2} \tag{24}$$

We note that Eq. (24) is identical to Eq. (20), which means that whenever there exist four extreme values of x, the trajectory intersects the plane of symmetry four times. When Eq. (24) is satisfied, two additional points of intersection can be found by substituting $\cos\theta_2$ from Eq. (22b) into Eq. (9). Since the y and z components of $\mathbf{P}$ depend only on $\cos\theta_2$, we conclude that the two additional points of intersection is a double point. This means the trajectory intersects itself and the node lies on the plane of symmetry as shown in Fig. 3. The coordinates of the node are

$$\mathbf{P}_{\text{node}} = \begin{bmatrix} 0 \\ s\alpha_3 \\ c\alpha_3 \end{bmatrix} \tag{25}$$

which is function of α_3 only.

Inequality (20) or (24) implies that whenever the twist angle α_3 is greater than the cone angle of the planet gear ($\alpha_p = \alpha_s = \alpha_2/2$) and less than its supplement, the locus of point P will intersect itself similar to the spur planetary gear train shown in Fig. 1. The equal sign results in a critical case where the node degenerates into a cusp. Therefore, the location of the cusp can also be expressed by Eq. (25). we have shown that the criterion for the existence of a cusp is similar to the planar case: the tracer point lies on the pitch cone of the planet gear or its mirror image about the origin.

Extrema of y

The extreme values of y can be found by equating the first derivative of the y-component in Eq. (9) to zero, i.e.

$$\frac{dy}{d\theta_2} = s\theta_2[2c\theta_2 s\alpha_3(1+c\alpha_2) + s\alpha_2 c\alpha_3] = 0 \tag{26}$$

Hence,

$$\theta_2 = 0 \text{ or } \pi \tag{27a}$$

or

$$\theta_2 = \cos^{-1}\left(-\frac{s\alpha_2 c\alpha_3}{2s\alpha_3(1+c\alpha_2)}\right) \tag{27b}$$

Equation (27a) implies that two extreme values of y occur at the same locations where the extreme values of z occur, and they are given by Eqs. (14) and (15), respectively. If the θ_2's derived from Eq. (27b) are real, then two additional points for extreme values of y exist. It can be shown that the y and z-coordinates of these two extreme points are given by Eqs. (12) and (11), respectively. Since the y and z components of $\mathbf{P}$ in Eq. (9) depend only on $\cos\theta_2$, the two extreme points have the same y and z coordinates, but different values of x.

Typical trajectories

Figure 4 shows some trajectories generated from a few typical bevel planetary gear trains. The shape of trajectory depends on the twist angles, α_2 and α_3. Generally, α_2 defines the maximum range in the latitudinal direction of trajectory, while α_3

defines the position of the node (or cusp). When $\alpha_2 = \pi/2$, the angle ψ_z between $\mathbf{P}_{z_{max}}$ and $\mathbf{P}_{z_{min}}$ is equal to π; when $\alpha_3 = \pi/2$, the trajectory is symmetric about the X-Y plane. The trajectory has a Fig. 8 shape if both sides of inequality in Eq. (24) are satisfied as shown in Figs. 4(*a*)-4(*d*). They are analogous to planar curves generated by a spur planetary gear train (Fig. 1), which are called limacons. A limacon is defined as the curve which has the form of $r = a - b \sin\theta$ or $r = a - b \cos\theta$, where r and θ are the parameters in polar coordinate system, and a and b are two constants. In the spherical motion, the third equation in Eq. (9) resembles the above relation. We shall name the trajectories traced by a tracer point on a bevel planetary gear train as spherical limacons. In summary, there are three types of spherical limacons: (*i*) when the twist angles do not satisfy Eq. (24), the trajectories become simply-connected curves; (*ii*) when one of the equality-sign in Eq. (24) is satisfied, the trajectory has a cusp; (*iii*) when the inequality in Eq. (24) is satisfied, the trajectory has a node. Figures 4(*e*) and (*g*) show two critical cases where the trajectories change to spherical cardioids, while Fig. 4(*f*) shows an example for which the left-hand-side of Eq. (24) is not satisfied.

5 Geometry of the Trajectory, Gear Ratio $n = 2$

For $n = 2$, Eq. (5) reduces to

$$\mathbf{P} = \begin{bmatrix} s\theta_2[2(1-s^2\theta_2)s\alpha_3(1+c\alpha_2) + s(\alpha_2-\alpha_3)] \\ c\theta_2[2(1-c^2\theta_2)s\alpha_3(1+c\alpha_2) - s(\alpha_2+\alpha_3)] \\ -c(2\theta_2)s\alpha_2 s\alpha_3 + c\alpha_2 c\alpha_3 \end{bmatrix} \tag{28}$$

Note that $\cos(2\theta_2) = 2\cos^2\theta_2 - 1 = 1 - 2\sin^2\theta_2$.

5.1 Geometric Description. Eliminating θ_2 from the second and third equations in Eq. (28), yields

$$y^2 = \frac{1+\zeta}{2}\,[s\alpha_3 - s\alpha_2 c\alpha_3 - s\alpha_3(1+c\alpha_2)\zeta]^2 \tag{29}$$

and eliminating θ_2 from the first and third equations, yields

$$x^2 = \frac{1-\zeta}{2}\,[s\alpha_3 + s\alpha_2 c\alpha_3 + s\alpha_3(1+c\alpha_2)\zeta]^2 \tag{30}$$

where $\zeta = (c\alpha_2 c\alpha_3 - z)/s\alpha_2 s\alpha_3$.

Equations (29) represents a cylinder with a cubic directrix in the Y-Z plane. Similarly, Eq. (30) also represents a cylinder with a cubic directrix in the X-Z plane. The cubic curve is called *Tschirnhausen's Cubic or l'Hospital's Cubic*. Hence, we may consider the trajectory as the intersection of a cubic cylinder and a unit sphere. From the two equations, it can be concluded that the curve has two planes of symmetry, the X-Z plane and the Y-Z plane.

5.2 Extrema, Nodes, and Cusps

Extrema of z

When the gear ratio is equal to two, the stationary condition for z coordinate is

$$\frac{dz}{d\theta_2} = 2s(2\theta_2)s\alpha_2 s\alpha_3 = 0 \tag{31}$$

Considering the second-order derivative of z, we conclude that, when $\theta_2 = -\pi/2$ and $\theta_2 = \pi/2$, z reaches its maximum, z_{max}. Substituting them into Eq. (28), we obtain, for $\theta_2 = -\pi/2$,

$$\mathbf{P}_{z_{max}} = \begin{bmatrix} -s(\alpha_2-\alpha_3) \\ 0 \\ c(\alpha_2-\alpha_3) \end{bmatrix} \tag{32}$$

and for $\theta_2 = \pi/2$,

$$\mathbf{P}_{z_{max}} = \begin{bmatrix} s(\alpha_2-\alpha_3) \\ 0 \\ c(\alpha_2-\alpha_3) \end{bmatrix} \tag{33}$$

Substituting $\theta_2 = 0$ into Eq. (28), we obtain the minimum of z

$$\mathbf{P}_{z_{min}} = \begin{bmatrix} 0 \\ -s(\alpha_2+\alpha_3) \\ c(\alpha_2+\alpha_3) \end{bmatrix} \tag{34}$$

and for $\theta_2 = \pi$

$$\mathbf{P}_{z_{min}} = \begin{bmatrix} 0 \\ s(\alpha_2+\alpha_3) \\ c(\alpha_2+\alpha_3) \end{bmatrix} \tag{35}$$

Note that the two vectors with maximal values of z lie on the X-Z plane, and are symmetric with respect to the Y-Z plane; while the two vectors with minimal values of z lie on the Y-Z plane, and are symmetric with respect to the X-Z plane.

Extrema of y

The stationary condition for y coordinate is found by letting

$$\frac{dy}{d\theta_2} = s\theta_2[-6s^2\theta_2 s\alpha_3(1+c\alpha_2) + 4s\alpha_3(1 + c\alpha_2) + s(\alpha_2+\alpha_3)] = 0 \tag{36}$$

The vectors with extreme values of y can be found by substituting the solutions of Eq. (36) into (28). There are at least two and at most six solutions to Eq. (36). When $\theta_2 = 0$ (or $\theta_2 = \pi$), the curve reaches its minimal (or maximal) value of y. Four additional solutions exist only if

$$0 \le \frac{2}{3} + \frac{s(\alpha_2+\alpha_3)}{6s\alpha_3(1+c\alpha_2)} \le 1 \tag{37}$$

Equation (37) can be simplified as

$$-2 \le \frac{s(\alpha_2+\alpha_3)}{2s\alpha_3(1+c\alpha_2)} \le 1 \tag{38}$$

Points of intersection at planes of symmetry

(*i*) The X-Z plane

The points of intersection at the X-Z plane can be obtained by equating the y component of Eq. (28) to zero, i.e.,

$$c\theta_2[2s^2\theta_2 s\alpha_3(1+c\alpha_2) - s(\alpha_2+\alpha_3)] = 0$$

Hence,

$$\theta_2 = -\pi/2 \text{ or } \pi/2 \tag{39a}$$

or

$$\theta_2 = \sin^{-1}\left[\pm\left(\frac{s(\alpha_2+\alpha_3)}{2s\alpha_3(1+c\alpha_2)}\right)^{\frac{1}{2}}\right] \tag{39b}$$

Equation (39*a*) implies that the trajectory intersects the X-Z plane at least twice at the locations where the maximal values of z occur. Equation (39*b*) yields four real solutions if

$$0 \le \frac{s(\alpha_2+\alpha_3)}{2s\alpha_3(1+c\alpha_2)} \le 1 \tag{40}$$

Since the denominator in Eq. (40) is always positive, the left-hand-side of Eq. (40) is satisfied when

$$\alpha_3 \le \pi - \alpha_2 \tag{41}$$

Substituting the relationship $\alpha_2 = \alpha_s + \alpha_p$ into the right-hand-side of Eq. (40) and after simplification, we obtain

$$\frac{s(\alpha_s+\alpha_p-\alpha_3)}{s\alpha_3} \le 2.$$

Comparing it with

$$\frac{\sin\alpha_s}{\sin\alpha_p} = 2,$$

we conclude that the right equality sign of Eq. (40) is satisfied

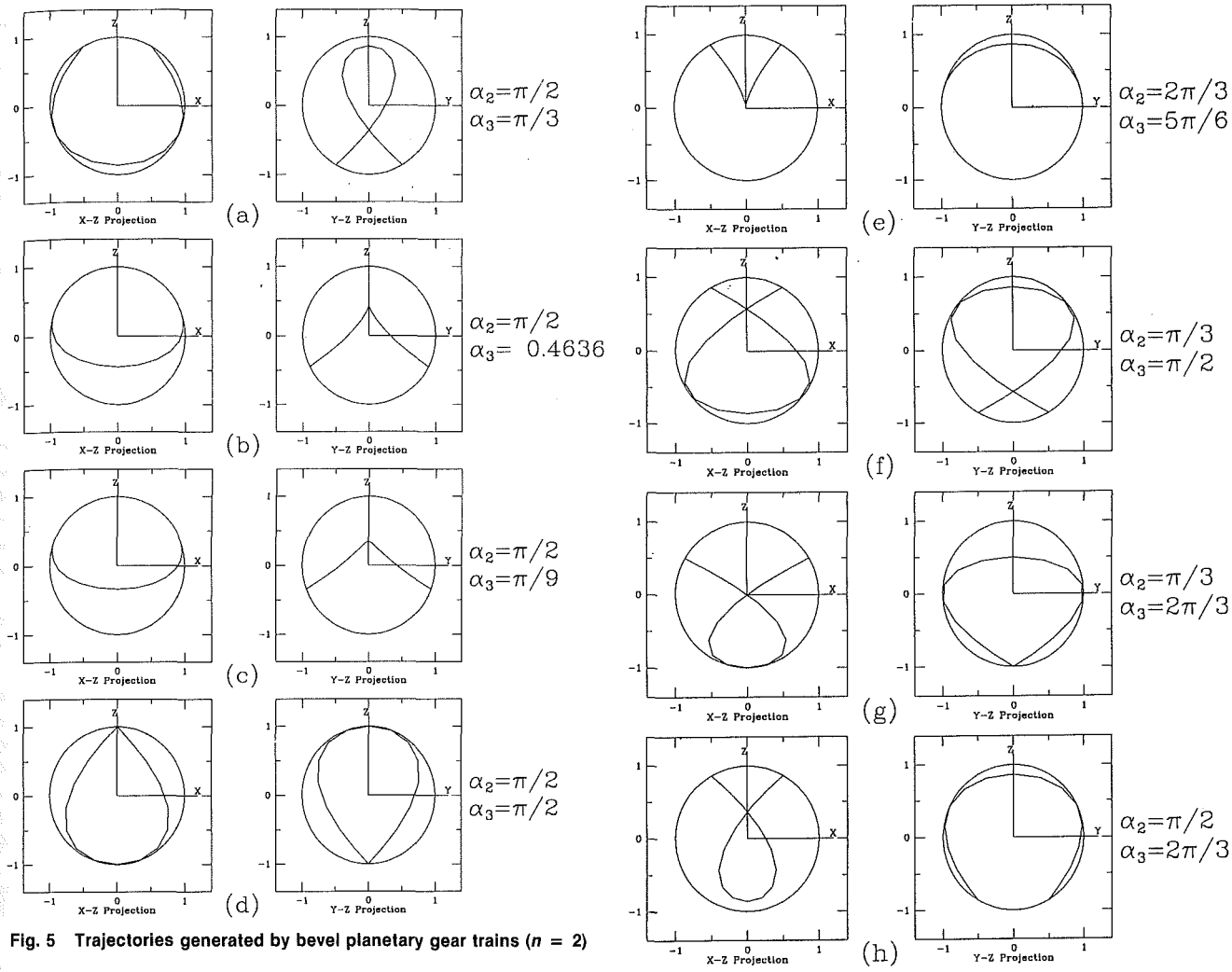

Fig. 5 Trajectories generated by bevel planetary gear trains (n = 2)

Fig. 5 (Continued)

when $\alpha_3 = \alpha_p$. For a given α_2, the function in Eq. (40) is a monotonically decreasing function of α_3 within the interval of $0 < \alpha_3 < \pi$. Hence, it follows that

$$\alpha_3 \geq \alpha_p \tag{42}$$

satisfies the right-hand-side of Eq. (40). Combining Eqs. (41) and (42), we obtain

$$\alpha_p \leq \alpha_3 \leq \pi - \alpha_2 \tag{43}$$

When Eq. (43) is satisfied, four additional points of intersection can be found by substituting sin θ_2 from Eq. (39b) into (28). Since the x and z components of **P** depend only on sin θ_2, we conclude that the four additional points of intersection are two double points (nodes). When the equal sign in Eq. (43) holds, the two nodes become two cusps.

Since Eq. (40) is a subset of Eq. (38), we can conclude that Eq. (43) also satisfy Eq. (38). Thus, when the trajectory intersects the X-Z plane six times, it has six extreme values of y.

(*ii*) The Y-Z plane

The points of intersection at the Y-Z plane can be obtained by equating the x component of Eq. (28) to zero, i.e.,

$$s\theta_2[2c^2\theta_2 s\alpha_3(1+c\alpha_2)+s(\alpha_2-\alpha_3)]=0$$

Hence,

$$\theta_2 = 0 \text{ or } \pi \tag{44a}$$

or

$$\theta_2 = \cos^{-1}\left[\pm\left(\frac{s(\alpha_3-\alpha_2)}{2s\alpha_3(1+c\alpha_2)}\right)^{\frac{1}{2}}\right] \tag{44b}$$

Equation (44a) implies that the trajectory intersects the Y-Z plane at least twice at the locations where the minimal values of z occur. Equation (44b) yields four real solutions if

$$0 \leq \frac{s(\alpha_3-\alpha_2)}{2s\alpha_3(1+c\alpha_2)} \leq 1 \tag{45}$$

The right-hand-side of Eq. (45) can be simplified as

$$-\frac{s(\alpha_s+\alpha_p+\alpha_3)}{s\alpha_3} \leq 2.$$

Comparing it with

$$\frac{\sin\alpha_s}{\sin\alpha_p} = 2,$$

we conclude that the right equality sign of Eq. (45) is satisfied when $\alpha_3 = \pi - \alpha_p$. For a given α_2, the function in Eq. (45) is a monotonically increasing function of α_3 within the interval of $0 < \alpha_3 < \pi$. Hence, it follows that

$$\alpha_3 \leq \pi - \alpha_p$$

satisfies the right-hand-side of Eq. (45). Hence, we can conclude that Eq. (45) will be satisfied if and only if

$$\alpha_2 \leq \alpha_3 \leq \pi - \alpha_p \tag{46}$$

Since the y and z components of $\mathbf{P}$ depend only on $\cos\theta_2$, we conclude that the four additional points of intersection are two double points (nodes).

Typical trajectories

Figure 5 shows some trajectories generated by bevel planetary gear trains having gear ratio equal to two. The curves are symmetric with respect to the X-Z and Y-Z planes. It should be noted that, given an α_2, the cone angle of the planet gear is given by

$$\alpha_p = \tan^{-1}\left(\frac{s\alpha_2}{c\alpha_2 + 2}\right).$$

Except for Fig. 5(c), all the other figures satisfy Eqs. (43) and/or (46). In Fig. 5(b), $\alpha_3 = \alpha_p$, the curve has two cusps; and in Fig. 5(e), $\alpha_3 = \pi - \alpha_p$, the curve also has two cusps. These curves are called *spherical nephroids*. Note that when Eq. (43) is satisfied, there will be a node or cusp on the Y-Z projection. Similarly, when Eq. (46) is satisfied, there will be a node or cusp on the X-Z projection. Table 1 shows the number of nodes and cusps of the trajectories shown in Fig. 5, and their relationship with Eqs. (43) and (46). It is concluded that, Eq. (43) or (46) should be satisfied for the existence of any nodes or cusps.

6 Instantaneous Screw Axis

For a bevel planetary gear train (Fig. 2), given $\dot{\theta}_2$, the angular velocity of link 3 with respect to the base link can be expressed in the $(XYZ)_1$ coordinate system as:

$$\begin{aligned} {}^1\omega_3 &= \dot{\theta}_2\mathbf{Z}_1 + \dot{\theta}_3\mathbf{Z}_2 \\ &= \dot{\theta}_2(\mathbf{Z}_1 + n\mathbf{Z}_2) \\ &= \dot{\theta}_2 \begin{bmatrix} ns\theta_2 s\alpha_2 \\ -nc\theta_2 s\alpha_2 \\ (1 + nc\alpha_2) \end{bmatrix} \end{aligned} \tag{47a}$$

The magnitude of ${}^1\omega_3$ is equal to $\dot{\theta}_2\sqrt{1+n^2+2nc\alpha_2}$, and its direction is along the line of $(\mathbf{Z}_1 + n\mathbf{Z}_2)$. Hence, the line passing through the origin and pointing in the direction of $(\mathbf{Z}_1 + n\mathbf{Z}_2)$ is the instantaneous screw axis for the motion of link 3 with respect to link 1. As θ_2 varies from 0 to 2π, the locus of the instantaneous screw axis form a screw cone with its vertex located at the origin. Similarly, the angular velocity vector of link 3 with respect to link 1 can also be expressed in the moving coordinate system $(XYZ)_2$ as:

$${}^2\omega_3 = \dot{\theta}_2 \begin{bmatrix} 0 \\ s\alpha_2 \\ c\alpha_2 + n \end{bmatrix} \tag{47b}$$

Equation (47b) implies that the instantaneous screw axis is fixed in the Y-Z plane of the carrier. Hence, it revolves around the fixed Z_1-axis as the carrier rotates about the first joint axis.

7 Summary

This paper discusses the trajectories of bevel planetary gear trains. Parametric equations for the trajectory are derived using 3×3 rotation matrix. We have shown that the trajectory generated by a tracer point on the planet of a bevel planetary gear train is analogous to that of a spur-gear train. When the gear ratio is equal to one, the trajectory is called spherical limacon or spherical cardioid depending on whether the tracer point lies on the outside or on the pitch cone of the planet gear. When the gear ratio is equal to two and the tracer point lies on the pitch cone of the planet gear, the curve is a spherical nephroid.

Table 1 The number of nodes or cusps and their relationship with Eqs. (43) and (46)

	Nodes	Cusps	$\alpha_p < \alpha_3 < \pi - \alpha_2$	$\alpha_2 < \alpha_3 < \pi - \alpha_p$
Fig. 5(a)	2	0	√	
Fig. 5(b)	0	2	$\alpha_3 = \alpha_p$	
Fig. 5(c)	0	0		
Fig. 5(d)	2	0	$\alpha_3 = \pi - \alpha_2$	$\alpha_3 = \alpha_2$
Fig. 5(e)	0	2		$\alpha_3 = \pi - \alpha_p$
Fig. 5(f)	4	0	√	√
Fig. 5(g)	3	0	$\alpha_3 = \pi - \alpha_2$	√
Fig. 5(h)	2	0		√

The geometric properties of these trajectories are investigated, including the planes of symmetry, extent of curves, number of nodes (cusps), and their locations. We have also shown that the criterion for existence of cusps can be interpreted geometrically as the tracer point being on the pitch cone of the planet gear or its image cone. From a geometric point of view, the spherical limacon can be interpreted as the intersection of a parabolic cylinder and a unit sphere; and the spherical nephroid can be interpreted as the intersection of Tschirnhausen's cylinder and a unit sphere.

This study is useful for a better understanding on the working space and singular points of gear-coupled robotic mechanisms. The results has been applied to the study of orientational workspace of three-DOF, four-jointed spherical wrist mechanisms (Lin and Tsai, 1991). It has been shown that the location of nodes and cups, plane of symmetry, cone angle, etc. have a dominate effect on the workspace of such gear coupled robotic mechanisms.

It is also anticipated that this study can be helpful in the development of spherical kinematics.

Acknowledgment

This work was supported in part by the U.S. Department of Energy under Grant DEF05-88ER13977 and in part by the NSF Engineering Research Centers Program, NSFD CDR 8803012. Such support does not constitute an endorsement by the supporting agencies of the views expressed in the paper.

References

Berger, M., and Gostiaux, B., 1988, *Differential Geometry: Manifolds, Curves, and Surfaces*, Springer-Verlag, New York.

Brieskorn, E., and Knörrer, H., 1986, *Plane Algebraic Curves*, Birkhäuser Boston Inc.

Butchart, J. H., 1945, "Some Properties of the Limacon and Cardioid," *Amer. Math. Monthly*, Vol. 52, pp. 384–387.

Denavit, J., and Hartenberg, R. S., 1955, "A Kinematic Notation for Lower Pair Mechanisms Based on Matrices," ASME *Journal of Applied Mechanics*, Vol. 77, pp. 215–221.

Hunt, K. H., 1978, *Kinematic Geometry of Mechanisms*, University Press, Oxford, Great Britain.

Jensen, P. W., 1965, "Cycloidal Gear Mechanisms," *Product Engineering*, Vol. 36, No. 13, pp. 82–88.

Lawrence, J. D., 1972, *A Catalog of Special Plane Curves*, Dover Publications, New York.

Lin, C. C., and Tsai, L. W., 1991, "The Workspace of Three-Degree-of-Freedom, Four-Jointed Spherical Wrist Mechanisms," Proc. of 1991 IEEE International Conference on Robotics and Automation, Sacramento, CA, Vol. 2, pp. 1548–1553.

McCarthy, J. P., 1945, "The Limacon and The Cardioid," *Math. Gazette*, Vol. 29, pp. 219–220.

Pollitt, E. P., 1960, "Some Applications of the Cycloid in Machine Design," ASME *Journal of Engineering for Industry*, Series B, Vol. 82, No. 3, pp. 407–414.

Spragg, D., and Tesar, D., 1971, "Generalized Cycloidal Motion," ASME *Journal of Engineering for Industry*, Series B, Vol. 93, No. 1, pp. 131–139.